

VUV Fourier-transform absorption study of the Lyman and Werner bands in D2

Arno de Lange, Gareth D. Dickenson, Edcel J. Salumbides, Wim Ubachs, Nelson de Oliveira et al.

Citation: *J. Chem. Phys.* **136**, 234310 (2012); doi: 10.1063/1.4726457

View online: <http://dx.doi.org/10.1063/1.4726457>

View Table of Contents: <http://jcp.aip.org/resource/1/JCPSA6/v136/i23>

Published by the [American Institute of Physics](http://www.aip.org).

Additional information on *J. Chem. Phys.*

Journal Homepage: <http://jcp.aip.org/>

Journal Information: http://jcp.aip.org/about/about_the_journal

Top downloads: http://jcp.aip.org/features/most_downloaded

Information for Authors: <http://jcp.aip.org/authors>

ADVERTISEMENT



Goodfellow
metals • ceramics • polymers • composites
70,000 products
450 different materials
small quantities fast

www.goodfellowusa.com

VUV Fourier-transform absorption study of the Lyman and Werner bands in D₂

Arno de Lange,^{1,a)} Gareth D. Dickenson,¹ Edcel J. Salumbides,¹ Wim Ubachs,¹ Nelson de Oliveira,² Denis Joyeux,² and Laurent Nahon²

¹*Institute for Lasers, Life and Biophotonics, VU University, De Boelelaan 1081, 1081 HV Amsterdam, The Netherlands*

²*Synchrotron Soleil, Orme des Merisiers, St Aubin BP 48, 91192, GIF sur Yvette Cedex, France*

(Received 13 April 2012; accepted 22 May 2012; published online 20 June 2012)

An extensive survey of the D₂ absorption spectrum has been performed with the high-resolution VUV Fourier-transform spectrometer employing synchrotron radiation. The frequency range of 90 000–119 000 cm⁻¹ covers the full depth of the potential wells of the $B^1\Sigma_u^+$, $B'^1\Sigma_u^+$, and $C^1\Pi_u$ electronic states up to the D(1s) + D(2ℓ) dissociation limit. Improved level energies of rovibrational levels have been determined up to respectively $v = 51$, $v = 13$, and $v = 20$. Highest resolution is achieved by probing absorption in a molecular gas jet with slit geometry, as well as in a liquid helium cooled static gas cell, resulting in line widths of ≈ 0.35 cm⁻¹. Extended calibration methods are employed to extract line positions of D₂ lines at absolute accuracies of 0.03 cm⁻¹. The $D^1\Pi_u$ and $B''^1\Sigma_u^+$ electronic states correlate with the D(1s) + D(3ℓ) dissociation limit, but support a few vibrational levels below the second dissociation limit, respectively, $v = 0-3$ and $v = 0-1$, and are also included in the presented study. The complete set of resulting level energies is the most comprehensive and accurate data set for D₂. The observations are compared with previous studies, both experimental and theoretical. © 2012 American Institute of Physics. [<http://dx.doi.org/10.1063/1.4726457>]

I. INTRODUCTION

Molecular hydrogen is the smallest neutral molecule and is as such a benchmark system for testing quantum mechanical calculations in molecules, starting from Born-Oppenheimer potentials, adiabatic and non-adiabatic corrections, leading to accurate predictions of level energies for all three natural isotopologues of hydrogen.¹ Recently, also high-order relativistic and quantum-electrodynamic effects, i.e., molecular Lamb shifts were included in the calculations, although limited to the $X^1\Sigma_g^+$ ground state.² For D₂ these calculations were subjected to test and confirmed in a measurement of the dissociation energy of the ground state³ at an accuracy level of < 0.001 cm⁻¹. For the electronically excited states of $^1\Sigma_u^+$ symmetry⁴ and $^1\Pi_u$ symmetry⁵ *ab initio* calculations have been performed, although at lower accuracy than for the ground state.

Due to the low nuclear masses in hydrogenic systems the validity of the Born-Oppenheimer approximation is only limited, less than in heavier molecules. Hence, isotopic effects are strong and the pronounced phenomena of mass-dependent adiabatic and non-adiabatic corrections can be well studied by comparing H₂, HD, and D₂, where HD exhibits additional effects of breaking of the inversion symmetry.⁶ For these reasons there is a continued interest in the investigation of the spectroscopy of hydrogen and its isotopomers, having started over a century ago by Lyman.⁷ In particular, the $B^1\Sigma_u^+$ – $X^1\Sigma_g^+$ Lyman and $C^1\Pi_u$ – $X^1\Sigma_g^+$ Werner systems have at-

tracted much attention, since these are the strongest, dipole-allowed, absorption systems originating from the $X^1\Sigma_g^+$ electronic ground state.

Spectroscopic studies on D₂ specifically bear relevance for the detailed investigation of thermonuclear fusion plasma reactors. For example, Hollmann *et al.* have detected extremely hot D₂ molecules in the DIII-D reactor from their spectroscopic signatures.⁸ Similarly Pospieszczyk *et al.* investigated various hydrogen molecular isotopomers in the JET fusion reactor.⁹

The first vacuum ultraviolet absorption spectrum of D₂ was studied by Beutler *et al.*¹⁰ in 1935 at relatively low resolution. From the 1960s, Herzberg and Monfils have studied its absorption spectrum over a wider range with a much higher accuracy, which led to the discovery of new electronic states ($B''^1\Sigma_u^+$, $D^1\Pi_u$, and $D''^1\Pi_u$).¹¹⁻¹³ In subsequent years Wilkinson,¹⁴ Bredohl and Herzberg,¹⁵ Dabrowski and Herzberg,¹⁶ Takezawa and Tanaka,¹⁷ and Larzillière *et al.*¹⁸ have further extended the spectral investigations using classical spectrometers.

Later, after the development of nonlinear optical techniques, tunable extreme ultraviolet (XUV) radiation from a laser-based source was used to yield improved accuracy in the spectroscopy of the D₂ Lyman and Werner bands.¹⁹ Over the years the accuracy has been further improved resulting in a highly accurate laser study by Roudjane *et al.*,²⁰ focusing on a low number of bands, which may be used for calibration purposes of subsequent studies, including the present one. The most accurate comprehensive investigations of the D₂ spectrum were conducted by Abgrall *et al.*²¹ and Roudjane *et al.*,^{22,23} both in emission and with spectrographs of 3 m and 10 m, respectively. Another extensive study is based on the

^{a)}Present address: SRON - Netherlands Institute for Space Research, Sorbonnelaan 2, 3584 CA Utrecht, The Netherlands. Electronic mail: A.de.Lange@sron.nl.

emission data by Dieke's laboratory group, collected over 30 years starting in the early 1930s. This dataset was analyzed and published by Freund *et al.*²⁴ Recently, Gabriel *et al.*²⁵ have investigated the Lyman bands of high rovibrationally excited D_2 molecules, extending the available data of level energies to high rotational states.

Here, we present a comprehensive absorption study of the D_2 spectrum, employing the high-resolution VUV Fourier-transform spectrometer at the SOLEIL synchrotron. All three electronic singlet states of *ungerade* symmetry correlating with the $D(1s) + D(2\ell)$ dissociation limit are investigated; the $B^1\Sigma_u^+$, $B'^1\Sigma_u^+$, and $C^1\Pi_u$ states. Rovibrational levels have been observed over the full potential well depths for vibrational levels up to, respectively, $v = 51$, $v = 13$, and $v = 20$, with an absolute accuracy of 0.03 cm^{-1} . Some electronic states converging to the $D(1s) + D(3\ell)$ dissociation limit, $D^1\Pi_u$ and $B''^1\Sigma_u^+$, also exhibit rovibrational levels below the second dissociation limit, which are also listed for completeness. Predissociation resonances above the $n = 2$ dissociation limit of D_2 have been published separately.²⁶

II. EXPERIMENTAL SETUP

The D_2 absorption spectra have been recorded in the gas phase at the synchrotron facility SOLEIL, where a vacuum ultraviolet (VUV) Fourier-Transform Spectrometer (FTS) (Refs. 27 and 28) has been installed as a permanent instrument on the VUV undulator-based Dichroïsme Et Spectroscopie par Interaction avec le Rayonnement Synchrotron (DESIRS) beamline.²⁹ This FTS provides a high resolving power of $\approx 10^6$ over the entire instrumental wavelength range of 40–180 nm covering the windowless regime of relevance for the present study. The undulator of the DESIRS beamline delivers broadband radiation with a bell-shaped spectrum, spanning $\approx 12\,000\text{ cm}^{-1}$, used as a continuum background feeding the FTS which central frequency is tuneable by changing the magnetic field of the undulator. The total frequency range investigated in the present study is 90 000–119 000 cm^{-1} and overlapping spectra are recorded for covering this wide frequency range.

Upstream of the FTS, the sample environment chamber is located, containing different types of gas-sample setups, upstream and downstream of which two similarly-sized holes ensure an efficient differential pumping with respect to the FTS chamber and the rest of the beamline. The FTS sample environment chamber is equipped with a free flow T-shaped gas cell containing the gas sample under quasi-static conditions. The cell is either cooled down with liquid nitrogen (L-N₂) or with liquid helium (L-He) to reduce Doppler broadening. This absorption facility was also used in a previous investigation on the Lyman and Werner bands of the HD molecule.³⁰ In the present study, a third type of measurement is performed in addition to the gas cell setup with two different coolants. The FTS is used to record absorption spectra from a D_2 molecular gas jet for the first time.

The free molecular jet is located downstream of the windowless gas cell (see Fig. 1 for experimental setup). The supersonic free expansion takes place in a separate chamber pumped continuously by a 500 L/s turbo-molecular pump.

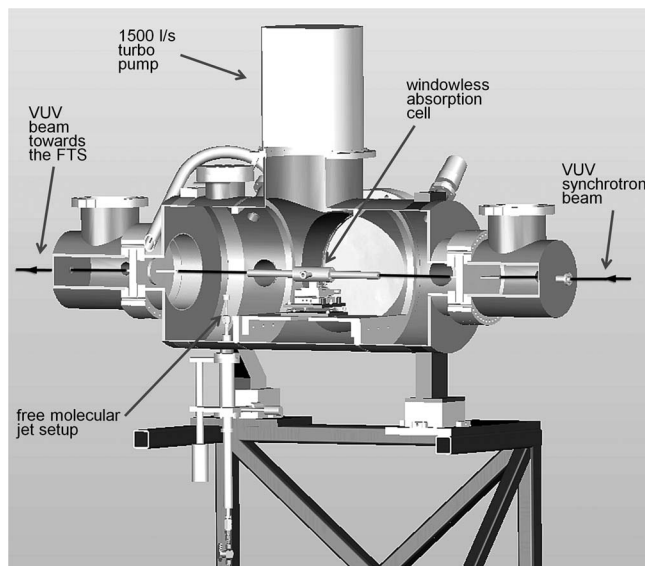


FIG. 1. The FTS branch gas sample chamber on the DESIRS beamline at the SOLEIL synchrotron. The chamber includes a windowless absorption cell that can be cooled down thanks to a continuous flow of L-N₂ or L-He, plus, a free molecular jet setup. For clarity, the separate differentially-pumped jet expansion chamber and the setup for cooling the windowless cell are omitted from the picture.

The synchrotron beam passes through two holes in the expansion chamber that approximately fit the dimensions of the beam to limit the vacuum conductance. A nozzle slit shape ($1\,000 \times 5\ \mu\text{m}^2$) is used, oriented so that the photon beam propagates along the slit length. The backing pressure has been set such that saturation on lines of interest is avoided; due to pumping limitations it is not possible to exceed backing pressures beyond 6 bar. It appears that the highest cold column density is observed when the photon beam crosses the molecular jet as close as possible to the nozzle position. Nevertheless, despite the two stages of differential pumping, background gas at room temperature can be seen on the absorption spectrum as a broad pedestal on which the narrow line is superimposed.

Figure 2 provides a view on the typical FT-spectral recordings, with two slightly shifted bell-shaped undulator profiles shown in the top panel, and two stages of zooming to show details of the individual absorption lines of D_2 . The black curves illustrate recordings with the molecular jet and the red curves illustrate measurements employing the L-N₂-cooled quasi-static gas cell. The figure shows that in the L-N₂-cooled cell configuration many more lines are discernable than in the jet configuration. However, the lines exhibit narrower profiles with the jet.

Under the three different experimental conditions, i.e., the L-N₂ and L-He cooled cell and the jet, different line widths are observed. These widths relate mainly to the resulting Doppler width, but also depend on the optical density at which the experiments are carried out. The data set covers, respectively, 326 lines for L-He cooled, 472 lines for L-N₂ cooled, and 284 lines for the jet configurations. These data pertain to the frequency range up to the second dissociation limit ($119\,030\text{ cm}^{-1}$), to exclude lines possibly broadened by predissociation. For all three cases the line width distribution

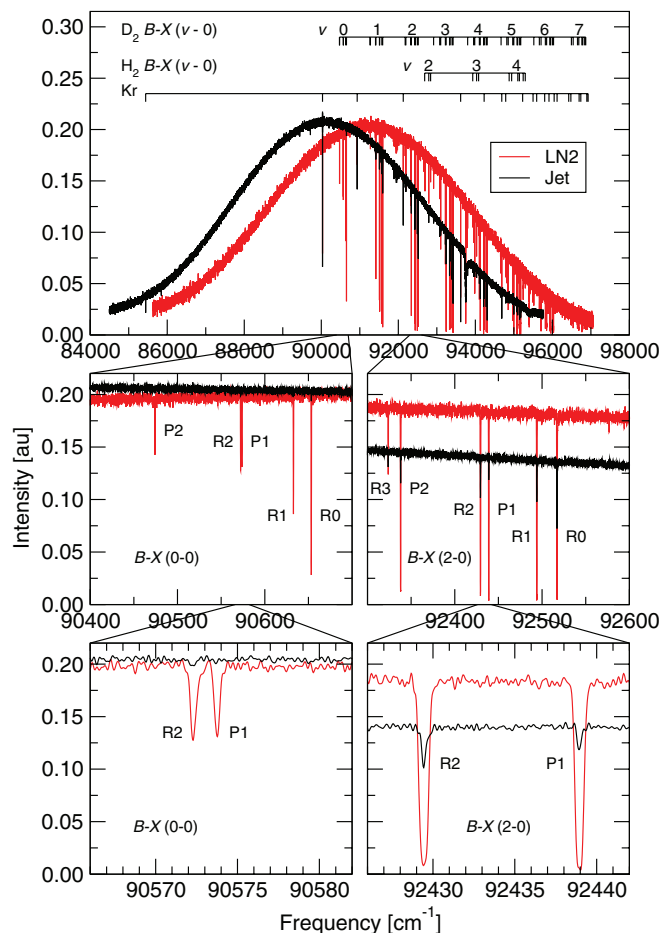


FIG. 2. D_2 absorption spectra recorded in a jet (black) and a cell cooled by liquid nitrogen (red). From the static gas cell setup many more lines are discernible. The lower panels zoom into two bands: $B^1\Sigma_u^+ - X^1\Sigma_g^+(0-0)$ (left) and $B^1\Sigma_u^+ - X^1\Sigma_g^+(2-0)$ (right). Note that a series of lines exciting Rydberg states of the Kr atom are included in some of the spectra; these lines originate from the gas filter used for eliminating harmonic radiation produced by the undulator. For further details see text.

is not normal and exhibits a shoulder towards higher widths; this is most pronounced for the L- N_2 case due to saturation effects. Discarding the saturated lines, the average means of the line widths, when fitting with a single Gaussian, are 0.35 cm^{-1} for the jet, 0.37 cm^{-1} for the L-He cooled cell, and 0.48 cm^{-1} for the L- N_2 cooled cell. The widths are a convolution of contributions of the instrument profile (a sinc-function of 0.16 cm^{-1} width related to the settings and travel arm of the FT-instrument), the effective Doppler width resulting from the inhomogeneously distributed outward diffusing gas in the cooled T-shaped cell, and a small additional broadening due to possible beam pointing instability during the FT-recordings. In the line width analysis above, the contribution of the background gas at room temperature is disregarded. Its effect is a broad pedestal on which the narrow(er) absorption line is superimposed and when not accounted for it effectively broadens the line. This effect is observed in particular in case of the jet.

In the recorded spectra, some H_2 lines are observed as well. The widths of these lines are 0.87 cm^{-1} , which is twice as broad as the unsaturated D_2 lines. This is due to a larger Doppler width, which stems mainly from the fact that the H_2

resides in the background gas at room temperature, but also from the lower mass of H_2 .

III. FREQUENCY CALIBRATION

The Fourier-transform spectra exhibit an internal frequency calibration derived directly from the interferogram sampling intervals and determined for each spectrum by an interferometric measurement using a stabilized helium-neon laser.^{27,28,30} Due to small alignment offsets of the helium-neon laser and the VUV beam relative directions, that may vary from run to run, the absolute calibration also varies for different runs, and can be improved upon by anchoring the spectra to several accurately known D_2 lines in addition to a few Xe and Kr lines that occur in the spectra, finding their origin in the gas filter used for attenuating the harmonics at short wavelengths produced in the undulator. Some 39 lines belonging to the $B^1\Sigma_u^+(v'=9-11) - X^1\Sigma_g^+(v''=0)$ and $C^1\Pi_u(v'=0) - X^1\Sigma_g^+(v''=0)$ systems, previously measured using an extreme ultraviolet laser instrument by Roudjane *et al.*²⁰ at an accuracy of 0.006 cm^{-1} , are used for this purpose. The Kr and Xe lines are taken from Refs. 31 and 32. The calibration procedure is repeated for each scan in order to remove any possible variation. In practice, the correction may vary slightly over long periods of time. After correction, the spread in the differences between the presently observed FT-line frequencies and the laser-based frequencies of Ref. 20 is 0.02 cm^{-1} , and this is taken as the statistical error for the present data set.

However, these calibration lines fall within $96\,000 - 100\,000\text{ cm}^{-1}$, a range that is only covered by the scans at low frequencies. Therefore, an extrapolation towards higher frequencies is required for the absolute calibration of the remaining scans. The absolute frequency scale of subsequent overlapping scans is adapted by overlaying a large number of lines (>30), yielding sufficient statistics to achieve a relative uncertainty in the frequency scale of $\approx 0.003\text{ cm}^{-1}$ between two adjacent scans. Towards higher frequencies, this procedure is applied multiple times, increasing the uncertainty with every step. The largest uncertainty pertains thus to the scan with the highest frequencies and amounts to 0.009 cm^{-1} . Based on this value, the systematic error is conservatively estimated to be 0.01 cm^{-1} for all scans. The uncertainty in the absolute frequencies for all lines is thus estimated at 0.03 cm^{-1} ; 0.02 cm^{-1} statistical plus 0.01 cm^{-1} systematic error.

In Fig. 3 electronic ground state combination differences are plotted for the line combinations $P(2) - R(0)$, $P(3) - R(1)$, and $P(4) - R(2)$, as measured in transitions to all vibrational levels in the $B^1\Sigma_u^+$, $C^1\Pi_u$, and $B'^1\Sigma_u^+$ states. Note that blended lines are excluded from this plot. The solid lines in these plots refer to the most accurate theoretical combination differences from Ref. 2, yielding $\Delta_{20} = 179.067\text{ cm}^{-1}$, $\Delta_{31} = 297.534\text{ cm}^{-1}$, and $\Delta_{42} = 414.649\text{ cm}^{-1}$. The observed combination differences agree very well with these theoretical values and the standard deviation for all differences is 0.025 cm^{-1} . This is in good agreement with the estimated statistical uncertainty of 0.02 cm^{-1} for a single line. In fact, it is even slightly lower than expected as the

TABLE I. Observed level energies for the $B^1\Sigma_u^+$ state in cm^{-1} , relative to the $X^1\Sigma_g^+$ ($v=0, J=0$) level. The uncertainties in the last digit are indicated in superscript and level energies that have been derived from blended lines, are listed with ^b. The highly accurate laser data by Roudjane *et al.*²⁰ are included in this table and marked with ^l.

v	$J=0$	$J=1$	$J=2$	$J=3$	$J=4$	$J=5$	$J=6$
0	90 633.47 ³	90 653.18 ³	90 692.52 ³	90 751.31 ³	90 829.14 ⁶
1	91 575.79 ³	91 594.78 ³	91 632.69 ³	91 689.32 ³	91 764.42 ³	91 857.61 ⁶	...
2	92 498.66 ³	92 517.03 ³	92 553.68 ³	92 608.45 ³	92 681.08 ³	92 771.33 ³	...
3	93 403.30 ³	93 421.10 ³	93 456.62 ³	93 509.71 ³	93 580.14 ³	93 667.65 ³	...
4	94 290.39 ³	94 307.67 ³	94 342.14 ³	94 393.70 ³	94 462.13 ³	94 547.11 ³	...
5	95 160.37 ³	95 177.16 ³	95 210.68 ³	95 260.82 ³	95 327.35 ³	95 410.03 ³	...
6	96 013.54 ³	96 029.88 ³	96 062.51 ³	96 111.30 ³	96 176.05 ³	96 256.52 ³	...
7	96 850.19 ³	96 866.12 ³	96 897.88 ³	96 945.41 ³	97 008.46 ³	97 086.85 ³	...
8	97 670.47 ³	97 685.98 ³	97 716.93 ³	97 763.23 ³	97 824.67 ³	97 901.09 ³	...
9	98 474.533 ^{7,l}	98 489.648 ^{6,l}	98 519.825 ^{6,l}	98 564.953 ^{6,l}	98 624.871 ^{7,l}	98 699.377 ^{6,l}	...
10	99 262.597 ^{6,l}	99 277.320 ^{6,l}	99 306.726 ^{7,l}	99 350.723 ^{6,l}	99 409.151 ^{6,l}	99 481.813 ^{7,l}	99 568.46 ⁶
11	100 034.805 ^{7,l}	100 049.180 ^{6,l}	100 077.890 ^{6,l}	100 120.825 ^{6,l}	100 177.850 ^{6,l}	100 248.771 ^{6,l}	...
12	100 791.34 ³	100 805.30 ³	100 833.31 ³	100 875.18 ³	100 930.78 ³	100 999.94 ³	101 082.46 ⁶
13	101 532.37 ³	101 546.06 ³	101 573.41 ³	101 614.35 ³	101 668.70 ³	101 736.41 ³	...
14	102 258.08 ³	102 271.41 ³	102 298.04 ³	102 337.91 ³	102 390.87 ³	102 456.77 ³	...
15	102 968.63 ³	102 981.69 ³	103 007.79 ³	103 046.89 ³	103 098.92 ³	103 164.24 ³	103 229.34 ⁶
16	103 664.22 ³	103 676.90 ³	103 702.28 ³	103 740.28 ³	103 790.78 ³	103 853.58 ³	...
17	104 344.98 ³	104 357.52 ³	104 382.58 ³	104 420.42 ³	104 475.47 ³	104 526.83 ³	...
18	105 011.18 ³	105 023.31 ³	105 047.54 ³	105 083.77 ³	105 131.91 ³
19	105 662.92 ³	105 676.38 ³	105 695.86 ³	105 732.17 ³	105 779.47 ³	105 838.11 ³	...
20	106 300.54 ³	106 312.10 ³	106 335.20 ³	106 369.80 ³	106 415.77 ³
21	106 924.02 ³	106 935.15 ³	106 957.46 ³	106 990.99 ³	107 035.67 ^b	107 091.36 ⁶	...
22	107 533.68 ³	107 544.75 ³	107 566.77 ³	107 599.89 ³	107 643.83 ³
23	108 129.68 ³	108 140.33 ³	108 161.69 ³	108 193.69 ³	108 236.34 ³	108 289.45 ³	...
24	108 712.16 ³	108 722.71 ³	108 743.81 ³	108 775.50 ³	108 817.76 ⁶
25	109 281.28 ³	109 291.47 ³	109 311.89 ³	109 342.45 ³	109 383.11 ³	109 433.81 ⁶	...
26	109 837.24 ³	109 847.38 ³	109 867.67 ³	109 898.28 ³
27	110 380.18 ³	110 389.92 ³	110 409.40 ³	110 438.56 ³
28	110 910.25 ³	110 920.20 ³	110 940.85 ³	110 955.32 ³	111 000.72 ³	111 049.15 ⁶	...
29	111 427.59 ³	111 436.87 ³	111 455.40 ⁶	111 483.28 ³	111 520.25 ³
30	111 932.28 ³	111 940.80 ³	111 958.39 ³	111 985.19 ³	112 021.03 ⁶
31	112 424.43 ³	112 433.30 ³	112 451.01 ³	112 477.57 ³	112 512.91 ⁶
32	112 904.16 ³	112 912.58 ³	112 929.54 ³	112 955.03 ³	112 989.05 ⁶
33	113 371.54 ^b	113 379.86 ³	113 396.76 ³	113 422.07 ³	113 455.91 ⁶
34	113 826.28 ³	113 834.38 ³	113 850.53 ³	113 874.79 ³
35	114 268.74 ³	114 276.76 ³	114 292.88 ³	114 317.09 ³
36	114 698.64 ³	114 706.32 ³	114 721.66 ³	114 744.65 ³	114 775.33 ⁶
37	115 115.91 ³	115 123.57 ³	115 138.96 ³	115 162.37 ³
38	115 520.27 ³	115 527.51 ³	115 542.00 ³	115 563.67 ³
39	115 911.40 ³	115 918.74 ³	115 933.71 ³	115 967.24 ^b	115 984.78 ^b
40	116 288.85 ³	116 295.63 ³	116 309.18 ³	116 329.49 ³	116 356.43 ⁶
41	116 651.94 ³	116 659.07 ³	116 678.24 ^b	116 685.29 ³	116 713.45 ^b
42	116 999.78 ³	117 006.05 ³	117 018.59 ³	117 037.35 ³
43	117 331.22 ³	117 338.29 ³	117 343.51 ³	117 363.91 ³	117 388.22 ⁶
44	117 644.59 ³	117 650.23 ³	117 661.57 ³	117 678.47 ³
45	117 937.59 ³	117 943.80 ³	117 948.20 ³	117 966.45 ³
46	118 207.17 ³	118 212.03 ³	118 222.21 ³	118 236.29 ³
47	118 448.94 ³	118 453.81 ³	118 465.33 ³	118 472.24 ³
48	118 656.86 ³	118 660.55 ³	118 668.01 ³	118 679.07 ³
49	118 822.43 ³	118 824.72 ³	118 830.72 ^b	118 839.59 ^b
50	118 934.57 ⁶	118 936.51 ³	118 940.29 ³	118 945.82 ⁶
51	118 988.95 ⁶	118 989.87 ³	118 991.74 ^b

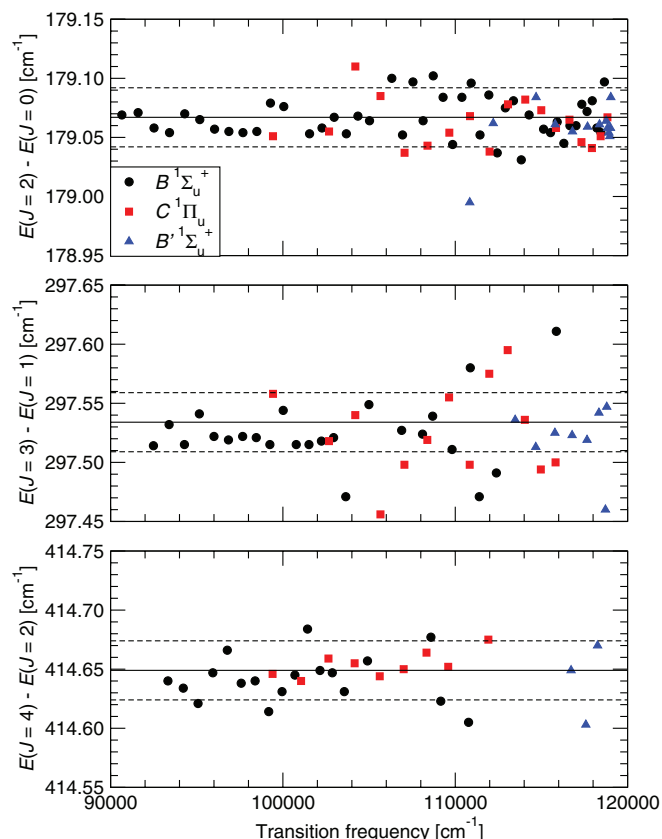


FIG. 3. The combination differences of various transition pairs from a wide range of vibrational levels in the $B^1\Sigma_u^+$ (black circles), $C^1\Pi_u$ (red squares), and $B'^1\Sigma_u^+$ (blue triangles) electronic states of D_2 . The following pairs are depicted; $P(2) - R(0)$ (upper panel), $P(3) - R(1)$ (central panel), and $P(4) - R(2)$ (lower panel). The solid lines correspond to the theoretical values of the combination differences, taken from Ref. 2. The dashed lines indicate the standard deviation of 0.025 cm^{-1} of all the differences. The transition frequencies refer to the R branch.

uncertainty in the combination differences from two transitions is $\sqrt{2} \times 0.02 = 0.03\text{ cm}^{-1}$. Note that only the statistical error is taken into account since the corresponding P and R transitions are sufficiently close in frequency to cancel any systematic errors in the combination differences.

TABLE II. Observed level energies for the $B'^1\Sigma_u^+$ state in cm^{-1} , relative to the $X^1\Sigma_g^+$ ($v=0, J=0$) level. The uncertainties in the last digit are indicated in superscript and level energies that have been derived from blended lines, are listed with ^b.

v	$J=0$	$J=1$	$J=2$	$J=3$	$J=4$	$J=5$
0	...	110 841.89 ³	110 894.39 ³	110 972.71 ³
1	112 180.87 ³	112 205.74 ³	112 255.40 ³	112 329.68 ³	112 428.29 ³	112 550.89 ⁶
2	113 467.04 ³	113 490.86 ³	113 538.45 ³	113 609.70 ³	113 704.43 ³	...
3	114 669.40 ³	114 690.74 ³	114 733.63 ³	114 798.35 ³	114 884.89 ^b	114 992.98 ³
4	115 779.82 ³	115 800.42 ³	115 841.55 ³	115 903.08 ³	115 984.78 ^b	116 086.36 ³
5	116 784.48 ³	116 803.71 ³	116 842.08 ³	116 899.49 ³	116 975.70 ^b	117 070.52 ³
6	117 659.28 ³	117 675.39 ³	117 707.81 ³	117 756.75 ³	117 821.99 ³	117 903.16 ³
7	118 357.31 ³	118 371.08 ³	118 398.42 ³	118 438.98 ³	118 492.18 ³	118 557.30 ⁶
8	118 754.82 ³	118 761.30 ³	118 773.70 ⁶	118 791.03 ³
9	118 838.52 ³	118 842.94 ³	118 852.22 ³	118 863.67 ³	118 881.06 ³	...
10	118 913.11 ³	118 916.30 ³	118 922.61 ³	118 931.99 ³	118 944.24 ⁶	...
11	118 966.66 ³	118 968.97 ³	118 973.56 ³	118 980.30 ³
12	119 003.47 ³	119 005.18 ³	119 008.49 ³	119 012.96 ³
13	119 027.27 ³	119 028.14 ³	119 029.62 ³

In addition, the scatter in line frequencies of strong D_2 lines, i.e., lines with a $S/N > 6$, that are observed in multiple runs is also 0.02 cm^{-1} , validating the statistical uncertainty estimate. However, for weaker lines (with $S/N < 6$) this scatter increases to 0.05 cm^{-1} , and hence the total uncertainty for these lines is estimated at 0.06 cm^{-1} .

To test the validity of the systematic error estimate of 0.01 cm^{-1} , the observed H_2 lines are compared with the highly accurate data by Bailly *et al.*³³ The standard deviation of these differences is 0.05 cm^{-1} , and is therefore more than twice as large as the observed scattering of 0.02 cm^{-1} in the D_2 lines. This can be explained by the fact that the observed H_2 lines are also more than twice as broad as the unsaturated D_2 lines. Because of this the H_2 lines are not used for the absolute calibration. The average of the 47 differences between the H_2 lines in the present study and the data by Bailly *et al.* is $0.005(7)\text{ cm}^{-1}$. Thus, the two datasets agree within this uncertainty and also the estimated systematic uncertainty of 0.01 cm^{-1} is consistent with this comparison.

IV. RESULTS

The dipole-allowed absorption spectrum of D_2 , in the range up to the $n=2$ dissociation limit, where narrow unpredissociated resonances are found, is recorded in absorption. Observed transition frequencies over the full depth of the potential wells of the $B^1\Sigma_u^+$, $B'^1\Sigma_u^+$, and $C^1\Pi_u$ electronic states, converging to the $n=2$ limit of D_2 are presented. The vibrational levels $v=0-51$ have been observed in the $B^1\Sigma_u^+$ state, $v=0-13$ in the $B'^1\Sigma_u^+$ state and $v=0-20$ in the $C^1\Pi_u$ state. In addition, the vibrational levels of the unpredissociated $D^1\Pi_u$ and $B''^1\Sigma_u^+$ states that lie below the second dissociation limit are presented as well; $v=0-3$ for $D^1\Pi_u$ and $v=0-1$ for $B''^1\Sigma_u^+$, respectively. Extensive lists of all observed transition frequencies are given in the supplementary material data depository of the American Institute of Physics.³⁴

Many of the measured lines have been observed before, albeit at lower accuracy. There are, however, a few levels probed for the first time. In case of the $B^1\Sigma_u^+$ state, Freund

TABLE III. Observed level energies for the $C^1\Pi_u$ state in cm^{-1} , relative to the $X^1\Sigma_g^+$ ($v=0, J=0$) level. The uncertainties in the last digit are indicated in superscript and level energies that have been derived from blended lines, are listed with ^b. The highly accurate laser data by Roudjane *et al.*²⁰ are included in this Table and marked with ^l.

v	$J=1$	$J=2$	$J=3$	$J=4$	$J=5$	$J=6$
	$C^1\Pi_u^+$					
0	99 424.957 ^{6,l}	99 486.942 ^{6,l}	99 579.584 ^{6,l}	99 702.495 ^{6,l}	99 855.174 ^{7,l}	...
1	101 085.41 ^b	101 145.17 ^b	101 234.54 ³	101 353.05 ³	101 500.09 ^b	101 675.10 ^b
2	102 677.96 ³	102 735.57 ³	102 821.63 ³	102 935.59 ³	103 076.56 ³	...
3	104 203.85 ³	104 259.09 ³	104 341.32 ³	104 446.30 ³	104 592.26 ³	...
4	105 662.55 ³	105 720.18 ³	105 798.95 ³	105 904.43 ³	106 035.49 ³	...
5	107 059.38 ³	107 110.86 ³	107 187.59 ³	107 289.11 ^b	107 414.91 ³	107 565.57 ^b
6	108 389.67 ³	108 438.85 ³	108 512.20 ³	108 609.17 ³	108 728.91 ³	...
7	109 655.36 ³	109 702.18 ³	109 771.80 ³	109 862.93 ³	109 965.30 ³	...
8	110 855.96 ³	110 899.27 ³	110 980.32 ³	111 061.62 ³	111 170.21 ³	...
9	111 992.28 ³	112 035.48 ³	112 099.47 ³	112 183.90 ³	112 288.36 ³	...
10	113 060.72 ³	113 101.37 ³	113 161.78 ³	113 241.53 ³
11	114 061.24 ³	114 099.35 ³	114 156.04 ³	114 230.56 ³
12	114 991.35 ³	115 026.78 ³	115 079.31 ³	115 146.75 ³
13	115 847.97 ³	115 880.38 ³	115 926.71 ³
14	116 626.94 ³	116 654.85 ³	116 709.53 ³	116 767.32 ⁶
15	117 322.89 ³	117 357.30 ³	117 395.93 ³	117 449.55 ⁶
16	117 929.64 ³	117 960.26 ³	117 994.06 ³	118 041.33 ³
17	118 437.01 ³	118 454.90 ³	118 491.68 ³
18	118 831.41 ³	118 847.08 ³	118 872.50 ⁶
19	119 085.91 ³	119 095.78 ³	119 111.03 ^b
	$C^1\Pi_u^-$					
0	99 424.672 ^{6,l}	99 486.108 ^{7,l}	99 577.958 ^{6,l}	99 699.867 ^{6,l}
1	101 085.05 ³	101 144.25 ³	101 232.72 ³	101 350.16 ³	101 495.96 ³	...
2	102 677.63 ³	102 734.61 ³	102 819.80 ³	102 932.83 ³	103 073.31 ³	...
3	104 203.55 ³	104 258.34 ³	104 340.28 ³	104 449.00 ³
4	105 663.72 ³	105 716.40 ³	105 795.13 ³	105 899.59 ³	106 029.24 ⁶	...
5	107 058.84 ³	107 110.86 ^b	107 184.93 ³	107 285.13 ³	107 409.59 ³	...
6	108 389.25 ³	108 437.70 ³	108 510.03 ³	108 606.02 ³	108 725.28 ³	...
7	109 655.05 ³	109 701.35 ³	109 770.53 ³	109 862.33 ³	109 976.27 ⁶	...
8	110 855.99 ³	110 900.14 ³	110 966.14 ³	111 053.67 ³
9	111 991.39 ³	112 033.41 ³	112 096.17 ³	112 179.39 ³	112 282.89 ^b	...
10	113 060.24 ³	113 100.05 ³	113 159.51 ³	113 238.38 ³
11	114 060.91 ³	114 098.46 ³	114 154.52 ³
12	114 991.15 ³	115 026.35 ³	115 078.82 ³
13	115 847.95 ^b	115 880.67 ³	115 929.49 ³
14	116 627.27 ³	116 657.35 ³	116 702.22 ³
15	117 323.76 ³	117 350.98 ³	117 391.54 ³	117 445.00 ³
16	117 930.35 ³	117 954.39 ³	117 990.23 ⁶
17	118 437.34 ³	118 457.76 ³	118 486.41 ^b
18	118 830.72 ^b	118 846.90 ³	118 870.76 ⁶
19	119 085.82 ³
20	119 157.00 ⁶

*et al.*²⁴ present level energies for the vibrational levels $v=48$ and $v=50$, but not $v=49$. This might have been caused by blending of lines; in our study the $R(1)$ and $R(2)$ transitions are blended, while the $R(0)$ and $P(1)$ transitions are well-resolved. Of the last observed $v=51$ vibrational level Dabrowski and Herzberg found the $R(0)$ transition,¹⁶ whereas in the present study the $R(0)$, $R(1)$, and $P(1)$ transitions have been observed. The observed vibrational levels $v=0-13$ in the $B^1\Sigma_u^+$ electronic state have all been observed before by Dabrowski and Herzberg,¹⁶ Freund *et al.*,²⁴ and Abgrall *et al.*²¹ In case of the $C^1\Pi_u$ electronic state, all vibrational levels $v=0-20$ were observed before by Dabrowski and Herzberg,¹⁶ while Freund

*et al.*²⁴ and Abgrall *et al.*²¹ observed only vibrational levels $v=0-18$.

The information content of the measured transition frequencies is condensed to values for the level energies. For those levels probed by multiple transitions, the uncertainty in the level energy is conservatively taken as the highest accuracy of these transitions, rather than an average. The highly accurate excitation energies of rotational levels in the $X^1\Sigma_g^+$ ground state are taken from Ref. 2. All resulting level energies for the five excited states of singlet and *ungerade* symmetry below the second dissociation limit of D_2 as probed in this study are listed in Tables I–V: Table I lists the data for the

TABLE IV. Observed level energies for the $D^1\Pi_u$ state in cm^{-1} , relative to the $X^1\Sigma_g^+$ ($v = 0, J = 0$) level. The uncertainties in the last digit are indicated in superscript.

v	$J = 1$	$J = 2$	$J = 3$	$J = 4$	$J = 5$
			$D^1\Pi_u^+$		
0	113 222.94 ³	113 283.38 ³	113 373.68 ³	113 493.18 ⁶	...
1	114 825.06 ³	114 885.13 ³	114 974.54 ³	115 092.29 ³	115 239.24 ³
2	116 359.51 ³	116 415.90 ³	116 500.02 ⁶	116 611.33 ³	116 748.96 ⁶
3	117 831.40 ³	117 886.79 ³	117 968.89 ³	118 076.91 ³	118 209.98 ³
			$D^1\Pi_u^-$		
0	113 222.42 ³	113 281.91 ³	113 370.85 ³	113 488.88 ⁶	...
1	114 823.44 ³	114 880.73 ³	114 966.37 ³
2	116 358.82 ³	116 413.95 ³	116 496.35 ³	116 605.73 ³	...
3	117 830.03 ³	117 883.05 ³	117 962.28 ³	118 067.44 ³	...

$B^1\Sigma_u^+$ state, Table II for the $B'^1\Sigma_u^+$ state, Table III for the $C^1\Pi_u$ state, Table IV for the $D^1\Pi_u$ state, and Table V for the $B''^1\Sigma_u^+$ state. In order to present the tables updated to the most accurate values, the highly accurate laser data of Roudjane *et al.*²⁰ are included in Tables I and III.

V. DISCUSSION

The present set of level energies comprises the most accurate comprehensive dataset for the five electronic states ($B^1\Sigma_u^+$, $B'^1\Sigma_u^+$, $B''^1\Sigma_u^+$, $C^1\Pi_u$, and $D^1\Pi_u$ states) of singlet and *ungerade* symmetry supporting bound levels below the $n = 2$ dissociation limit in D_2 . It is of interest to compare these accurate determinations of experimental level energies with those from previous studies and to those predicted by theory. It is noted that a comparison with the accurate laser data by Roudjane *et al.*²⁰ is made implicitly since those data are used for calibration of the presently recorded spectra.

First a comparison is made with the laser data by Hinnen *et al.*,¹⁹ a comprehensive data set with claimed accuracies of $0.03\text{--}0.08\text{ cm}^{-1}$. It is noted that the XUV-laser system in this study is based on a pulsed dye laser (PDL) system as opposed to the pulsed dye amplifier (PDA) system used by Roudjane *et al.*²⁰ The instrument width with the PDL is much larger than with the PDA, and subsequently leads to a lower accuracy. For technical details see also Ref. 35. The comparison between the present study and the data by Hinnen is shown in Fig. 4.

The solid line is the averaged difference and amounts to -0.10 cm^{-1} , with the dashed lines the $1\sigma = 0.05\text{ cm}^{-1}$ spread in the differences. The values by Hinnen *et al.* are thus systematically higher than in the present study. A similar difference (-0.07 cm^{-1}) has also been observed in the case of H_2 as pointed out by Philip *et al.*³⁶ It is therefore believed that

this systematic offset is due to the PDL-laser setup and the calibration procedure used in Ref. 19.

In the work of Abgrall *et al.*²¹ a semi-empirical calculation is performed including non-adiabatic interaction effects in a four-state analysis for the (e)-parity levels ($B^1\Sigma_u^+$, $B'^1\Sigma_u^+$, $C^1\Pi_u^+$, and $D^1\Pi_u^+$ states); the (f)-parity levels can be treated separately in a two-state analysis involving $C^1\Pi_u^-$ and $D^1\Pi_u^-$ states. These calculations were based on the Born-Oppenheimer potential curves by Dressler and Wolniewicz³⁷ and the *ab initio* calculations of the non-adiabatic couplings.^{38,39} In a study of the emission spectrum of D_2 , the existing potentials were semi-empirically optimized by fitting to line intensities and line positions in the spectrum, resulting in a slightly deviating potential energy curve.²¹ Experimental line positions were taken from the analysis by Freund *et al.*,²⁴ who analysed the extensive emission dataset from Dieke's laboratory group. In Fig. 5 the differences between the experimental level energies, as determined in the current study, with respect to the semi-empirical calculations by Abgrall *et al.*,²¹ are shown for the $B^1\Sigma_u^+$, $B'^1\Sigma_u^+$, $C^1\Pi_u$, and $D^1\Pi_u$ electronic states. The systematic deviation of 0.2 cm^{-1} between the present experimental results and the calculations in the lower frequency range ($<100\,000\text{ cm}^{-1}$) is ascribed to an offset in the experimental values in the emission study; the theoretical values in Ref. 21 are adapted to the experimental ones via a fit of the potential. An absolute calibration uncertainty of 0.2 cm^{-1} is not surprising for a classical spectrometer study. The deviation of about 0.15 cm^{-1} in the frequency range $105\,000\text{--}110\,000\text{ cm}^{-1}$ between levels pertaining to $B^1\Sigma_u^+$ and $C^1\Pi_u$ states is more surprising, since these points derive from the same part of the spectrum and relate to relative errors. The scatter in the data points for the $C^1\Pi_u$ state is most likely to be ascribed to non-adiabatic interactions with the $B^1\Sigma_u^+$ state, modeled only to a certain extent. In the frequency range $>113\,000\text{ cm}^{-1}$ the

TABLE V. Observed level energies for the $B''^1\Sigma_u^+$ state in cm^{-1} , relative to the $X^1\Sigma_g^+$ ($v = 0, J = 0$) level. The uncertainties in the last digit are indicated in superscript.

v	$J = 0$	$J = 1$	$J = 2$	$J = 3$	$J = 4$
0	117 197.17 ³	117 224.14 ³	117 278.03 ³	117 358.68 ³	117 465.87 ⁶
1	118 688.02 ³	118 714.41 ³	118 767.09 ³	118 845.98 ³	118 950.81 ³

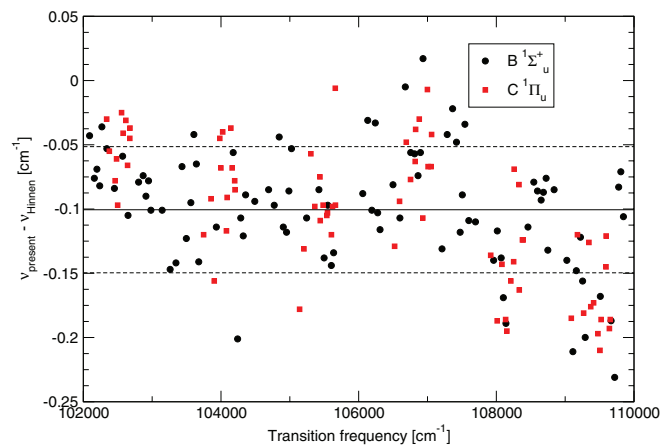


FIG. 4. Deviations between observed transitions in the present study and the observed transition frequencies by Hinnen *et al.*¹⁹ Black circles refer to transitions to the $B^1\Sigma_u^+$ state, whereas the red squares pertain to the $C^1\Pi_u$ state.

scatter in the data points becomes much larger (even as large as ± 0.2 cm^{-1}); here the modeling of non-adiabatic interactions between the four states of (e) symmetry is the limiting factor. This conclusion is supported by the fact that the levels pertaining to the $D^1\Pi_u^-$ state (f-symmetry) show much less spread per vibrational level than for the $D^1\Pi_u^+$ state; indeed the $D^1\Pi_u^-$ state only interacts with the $C^1\Pi_u^+$ state, while the $D^1\Pi_u^+$ state is part of a four state interaction. In fact, in the region $> 117\,000$ cm^{-1} the $B''^1\Sigma_u^+$ state perturbs the (e)-levels and is not accounted for in the theoretical model. Over the whole frequency range, the $B^1\Sigma_u^+$ state shows hardly any scatter in the data points, which can be interpreted that this state is only weakly perturbed by other states, apart from a few incidental local interactions. There are some outliers in

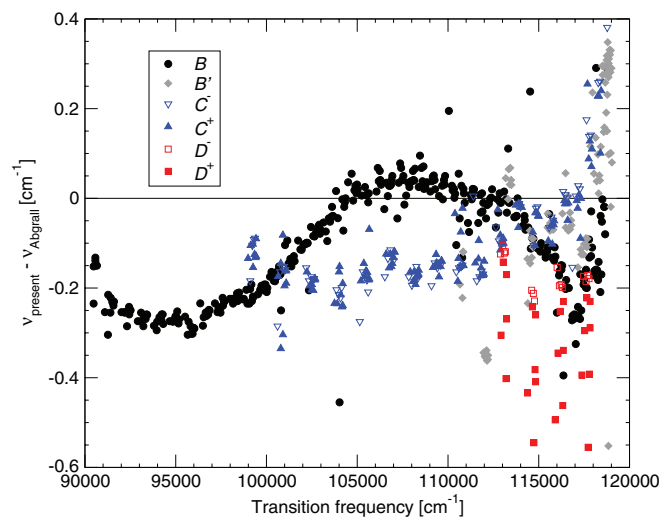


FIG. 5. Deviations between observed level energies in the present study and the semi-empirically calculated values by Abgrall *et al.*²¹ The black circles refer to the $B^1\Sigma_u^+$ electronic state, the grey diamonds to $B'^1\Sigma_u^+$, the blue triangles to $C^1\Pi_u$, and the red squares to $D^1\Pi_u$. The open triangles and squares pertain correspond, respectively, to the $C^1\Pi_u^-$ and $D^1\Pi_u^-$ electronic states, whereas the filled shapes to $C^1\Pi_u^+$ and $D^1\Pi_u^+$. The solid black line at 0 cm^{-1} is to guide the eye, and clearly shows that the values in the present study are mostly lower than those by Abgrall *et al.*²¹

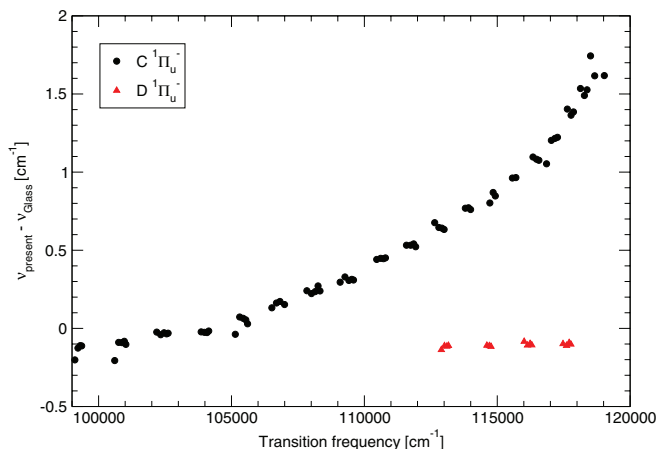


FIG. 6. Deviations between observed level energies in the present study and those of the MQDT-calculations by Glass-Maujean *et al.*⁴¹ The black circles correspond to Q transitions to the $C^1\Pi_u^-$ electronic state and the red triangles to $D^1\Pi_u^-$.

the differences between the dataset by Abgrall *et al.*²¹ and the present study. However, almost all either pertain to blended lines in the present study, or show a similar difference between the fitted values by Abgrall *et al.*²¹ and the measured transition frequencies as given by Freund *et al.*²⁴ This indicates that the modeled spectra do not fully capture all level interactions.

In Fig. 6 a comparison is made between the presently observed data and those obtained from another theoretical framework, the multi-channel quantum defect (MQDT)-formalism. The MQDT-formalism was developed by Jungen and Atabek⁴⁰ to describe the level structure of $C^1\Pi_u$ and $D^1\Pi_u$ states of the hydrogen molecule. This framework has recently been further refined by Glass-Maujean *et al.* and compared with accurate data on emission in hydrogen and deuterium, focusing on $C^1\Pi_u^-$ and $D^1\Pi_u^-$ levels.⁴¹ The MQDT-calculations are in good agreement with the present measurements, and can be seen to be accurate to within 1.5 cm^{-1} for both the $C^1\Pi_u^-$ and $D^1\Pi_u^-$ electronic states. For low vibrational levels, occurring deeply in the potential wells, the differences are much smaller, and are only 0.1 – 0.2 cm^{-1} .

VI. CONCLUSION

High resolution spectra of the D_2 molecule have been recorded with the VUV Fourier-transform spectrometer at the DESIRS beamline at the SOLEIL synchrotron. For the first time a slit jet geometry was combined with the VUV-FTS to achieve a spectral resolution of 0.35 cm^{-1} , while spectra of similar quality were obtained employing a liquid-He cooled quasi-static gas cell. The present study delivers the most comprehensive and accurate data set for the $B^1\Sigma_u^+$, $B'^1\Sigma_u^+$, and $C^1\Pi_u$ electronic states in D_2 covering the entire depth of the potential wells below the $n = 2$ dissociation limit. In addition, the sharp unpredissociated levels of the $D^1\Pi_u$ and $B''^1\Sigma_u^+$ states are included. Line positions are determined, and level energies extracted, at an absolute accuracy of 0.03 cm^{-1} , which corresponds to a fractional uncertainty of 3×10^{-7} .

ACKNOWLEDGMENTS

The authors would like to thank Dr. Alan Heays for fruitful discussions on the data analysis. The Netherlands Foundation for Fundamental Research of Matter (FOM) is gratefully acknowledged for financial support. We are grateful to the general staff of SOLEIL for running the facility and, in particular, to Jean-François Gil for his technical help with the sample environment chamber.

- ¹L. Wolniewicz, *J. Chem. Phys.* **103**, 1792 (1995).
- ²J. Komasa, K. Piszczatowski, G. Łach, M. Przybytek, B. Jeziorski, and K. Pachucki, *J. Chem. Theory Comput.* **7**, 3105 (2011).
- ³J. Liu, D. Sprecher, C. Jungen, W. Ubachs, and F. Merkt, *J. Chem. Phys.* **132**, 154301 (2010).
- ⁴G. Staszewska and L. Wolniewicz, *J. Mol. Spectrosc.* **212**, 208 (2002).
- ⁵L. Wolniewicz and G. Staszewska, *J. Mol. Spectrosc.* **220**, 45 (2003).
- ⁶A. de Lange, E. Reinhold, and W. Ubachs, *Int. Rev. Phys. Chem.* **21**, 257 (2002).
- ⁷T. Lyman, *Astrophys. J.* **23**, 181 (1906).
- ⁸E. M. Hollmann, S. Brezinsek, N. H. Brooks, M. Groth, A. G. McLean, A. Y. Pigarov, and D. L. Rudakov, *Plasma Phys. Controlled Fusion* **48**, 1165 (2006).
- ⁹A. Pospieszczyk, S. Brezinsek, A. Meigs, P. Mertens, G. Sergienko, and M. Stamp, *J. Nucl. Mater.* **363**, 811 (2007).
- ¹⁰H. Beutler, A. Deubner, and H. O. Jünger, *Z. Phys.* **98**, 181 (1935).
- ¹¹G. Herzberg and A. Monfils, *J. Mol. Spectrosc.* **5**, 482 (1960).
- ¹²A. Monfils, *J. Mol. Spectrosc.* **15**, 265 (1965).
- ¹³A. Monfils, *J. Mol. Spectrosc.* **25**, 513 (1968).
- ¹⁴P. G. Wilkinson, *Can. J. Phys.* **46**, 1225 (1968).
- ¹⁵H. Bredohl and G. Herzberg, *Can. J. Phys.* **51**, 867 (1973).
- ¹⁶I. Dabrowski and G. Herzberg, *Can. J. Phys.* **52**, 1110 (1974).
- ¹⁷S. Takezawa and Y. Tanaka, *J. Mol. Spectrosc.* **54**, 379 (1975).
- ¹⁸M. Larzillière, F. Launay, and J.-Y. Roncin, *J. Phys. (Paris)* **41**, 1431 (1980).
- ¹⁹P. C. Hinnen, W. Hogervorst, S. Stolte, and W. Ubachs, *Can. J. Phys.* **72**, 1032 (1994).
- ²⁰M. Roudjane, T. I. Ivanov, M. O. Vieitez, C. A. de Lange, W.-Ü. L. Tchang-Brillet, and W. Ubachs, *Mol. Phys.* **106**, 1193 (2008).
- ²¹H. Abgrall, E. Roueff, X. Liu, D. E. Shemansky, and G. K. James, *J. Phys. B* **32**, 3813 (1999).
- ²²M. Roudjane, F. Launay, and W.-Ü. L. Tchang-Brillet, *J. Chem. Phys.* **125**, 214305 (2006).
- ²³M. Roudjane, W.-Ü. L. Tchang-Brillet, and F. Launay, *J. Chem. Phys.* **127**, 054307 (2007).
- ²⁴R. S. Freund, J. A. Schiavone, and H. M. Crosswhite, *J. Phys. Chem. Ref. Data* **14**, 235 (1985).
- ²⁵O. Gabriel, J. J. A. van den Dungen, E. Roueff, H. Abgrall, and R. Engeln, *J. Mol. Spectrosc.* **253**, 64 (2009).
- ²⁶G. D. Dickenson, T. I. Ivanov, W. Ubachs, M. Roudjane, N. de Oliveira, D. Joyeux, L. Nahon, W.-Ü. L. Tchang-Brillet, M. Glass-Maujean, H. Schmoranzler *et al.*, *Mol. Phys.* **109**, 2693 (2011).
- ²⁷N. de Oliveira, D. Joyeux, D. Phalippou, J. C. Rodier, F. Polack, M. Vervloet, and L. Nahon, *Rev. Sci. Instrum.* **80**, 043101 (2009).
- ²⁸N. de Oliveira, M. Roudjane, D. Joyeux, D. Phalippou, J. C. Rodier, and L. Nahon, *Nature Photon.* **5**, 149 (2011).
- ²⁹L. Nahon, N. de Oliveira, G. Garcia, J. F. Gil, B. Pilette, O. Marcouillé, B. Lagarde, and F. Polack, "DESIRS: A state-of-the-art VUV beamline featuring high resolution and variable polarization for spectroscopy and dichroism at SOLEIL," *J. Synchrotron Rad.* (in press).
- ³⁰T. I. Ivanov, G. D. Dickenson, N. de Oliveira, M. Roudjane, D. Joyeux, L. Nahon, W.-Ü. L. Tchang-Brillet, and W. Ubachs, *Mol. Phys.* **108**, 771 (2010).
- ³¹F. Brandi, W. Hogervorst, and W. Ubachs, *J. Phys. B* **35**, 1071 (2002).
- ³²F. Brandi, I. Velchev, W. Hogervorst, and W. Ubachs, *Phys. Rev. A* **64**, 032505 (2001).
- ³³D. Bailly, E. J. Salumbides, M. Vervloet, and W. Ubachs, *Mol. Phys.* **108**, 827 (2010).
- ³⁴See supplementary material at <http://dx.doi.org/10.1063/1.4726457> for all measured transition frequencies.
- ³⁵W. Ubachs, K. S. E. Eikema, W. Hogervorst, and P. C. Cacciani, *J. Opt. Soc. Am. B* **14**, 2469 (1997).
- ³⁶J. Philip, J. P. Sprengers, T. Pielage, C. A. de Lange, W. Ubachs, and E. Reinhold, *Can. J. Chem.* **82**, 713 (2004).
- ³⁷K. Dressler and L. Wolniewicz, *J. Chem. Phys.* **85**, 2821 (1986).
- ³⁸P. Senn, P. Quadrelli, and K. Dressler, *J. Chem. Phys.* **89**, 7401 (1988).
- ³⁹L. Wolniewicz and K. Dressler, *J. Chem. Phys.* **96**, 6053 (1992).
- ⁴⁰C. Jungen and O. Atabek, *J. Chem. Phys.* **66**, 5584 (1977).
- ⁴¹M. Glass-Maujean, C. Jungen, M. Roudjane, and W.-Ü. L. Tchang-Brillet, *J. Chem. Phys.* **134**, 204305 (2011).